Research in Astron. Astrophys. **2013** Vol. **13** No. **5**, 557–570
http://www.raa-journal.org *http://www.iop.org/journals/raa*

Research in Astronomy and Astrophysics

Sequential clustering of star formations in IC 1396 *

Ya-Fang Huang and Jin-Zeng Li

National Astronomical Observatories, Chinese Academy of Sciences, Beijing 100012, China; *huangyf@nao.cas.cn*

Received 2012 September 1; accepted 2012 December 6

Abstract We present a comprehensive study of the H II region IC 1396 and its star forming activity, in which multi-wavelength data ranging from the optical to the near- and far-infrared were employed. The surface density distribution of all the 2MASS sources with a certain detection toward IC 1396 indicates the existence of a compact cluster spatially consistent with the position of the exciting source of the H II region, HD 206267. The spatial distribution of the sources with excessive infrared emission, selected based on archived 2MASS data, reveals the existence of four sub-clusters in this region. One is associated with the open cluster Trumpler 37. The other three are found to be spatially coincident with the bright rims of the H II region. All the sources with excessive emission in the near infrared are cross-identified with AKARI IRC data. An analysis of the spectral energy distributions (SEDs) of the resultant sample leads to the identification of eight CLASS I, 15 CLASS II and 15 CLASS III sources in IC 1396. Optical identification of the sample sources with R magnitudes brighter than 17 mag corroborates the results from the SED analysis. Based on the spatial distribution of the infrared young stellar objects at different evolutionary stages, the surrounding sub-clusters located in the bright rims are believed to be younger than the central one. This is consistent with a scenario of sequential star formation in this region. Imaging data of a dark patch in IC 1396 by Herschel SPIRE, on the other hand, indicate the presence of two far-infrared cores in LDN 1111, which are likely to be a new generation of protostellar objects in formation. So we infer that the star formation process in this H II region was not continuous but rather episodic.

Key words: techniques: photometric — stars: formation — stars: pre–main sequence — infrared: stars

1 INTRODUCTION

Molecular clouds (Lada & Lada 2003) are active sites of clustered star formation and the formation of massive stars. Cepheus OB2 (Cep OB2), known to be located in the local (Orion) spiral arm, is divided into two subgroups (Simonson 1968): (1) Cep OB2a contains 75 O- and B-stars that are spread over a large area, between $100^\circ < l < 106^\circ$ and $+2^\circ < b < +8^\circ$. It has an estimated age of 6–7 Myr; (2) Cep OB2b, namely Trumpler 37 (Tr 37), has an age of 3 Myr and is among the youngest known open clusters (Kun et al. 2008).

∗ Supported by the National Natural Science Foundation of China.

Tr 37 is associated with the shell-like H II region, IC 1396. IC 1396 is located at the southwest tip of Cep OB2, just above the galactic plane at $l = 99.3^\circ$ and $b = 3.74^\circ$. This H II region is mainly excited by the central O6 star HD 206267. As an extended H II region ($\sim 3^\circ$) at about 800 pc (Simonson 1968), it harbors a significant population of Pre-Main Sequence stars (PMS) with low- to intermediate masses.

Large-scale observations of IC 1396 with rotational CO lines (Patel et al. 1995; Weikard et al. 1996) and the associated radio map (Matthews et al. 1980; Wendker & Baars 1980) have uncovered a scattered, ring-like structure. The appearance of the H II region is dominated by a high degree of fragmentation into many dark and bright-rimmed globules. Near-infrared (IR) observations of IC 1396 and extinction maps obtained by data from the Two Micron All Sky Survey (2MASS) reveal star-formation activity and large numbers of globules in this region (Froebrich et al. 2005). Some of the densest regions in IC 1396 have already been investigated in detail (IC 1396N: Neri et al. (2007); Choudhury et al. (2010); Getman et al. (2007). IC 1396W: Froebrich & Scholz (2003). IC 1396A: Reach et al. (2004, 2009)). More and more young stellar objects (YSOs) have been detected with Chandra, Spitzer and other bands (Mercer et al. 2009; Barentsen et al. 2011; Nakano et al. 2012).

Infrared Astronomical Satellite (IRAS) all sky survey covers more than 96% of the entire sky in four photometric bands at 12, 25, 60 and 100 μm. The IRAS Sky Survey Atlas (ISSA) has shown that a census of mid- and far-IR is essential for studying objects embedded in dust in IC 1396. 2MASS is the first near-IR survey that has made uniformly calibrated observations of the entire sky in the J $(1.25\ \mu\mathrm{m})$, H $(1.65\,\mu\mathrm{m})$, and K_S $(2.16\ \mu\mathrm{m})$ bands with a pixel size of $2.0''$. Sources brighter than about 1 mJy in each band were detected with a signal-to-noise ratio greater than 10, which leads to a photometric completeness to 15.9, 15.0, and 14.3 mag for each band, respectively, in unconfused regions. For details about the 2MASS survey and the 2MASS Point Source Catalog (PSC), please consult the 2MASS Explanatory Supplement[1].

Large area surveys in near-IR and 2MASS provide an opportunity to investigate the sources with excessive emission, but their mid- and far-IR counterparts are rare and hard to uniquely identify in the IRAS catalog, preventing an efficient search of objects surrounded by dust. AKARI, a satellite operated by Japan, fulfills the need for a new mid- and far-IR whole sky survey with better sensitivity and a higher spatial resolution. Since its launch on 2006 February 21, AKARI has mapped 96% of the entire sky in mid and far-IR using two onboard instruments: the Infrared Camera (IRC; Onaka et al. 2007) and the Far-Infrared Surveyor (FIS; Kawada et al. 2007). The FIS has swept about 94% of the whole sky more than twice at 65, 90, 140, and 160 μm wavebands, while IRC has swept more than 90% of the whole sky more than twice using two filter bands centered at 9 μm (*S9W*, 7–12 μm) and 18 μm (*L18W*, 14–25 μm) (Ishihara et al. 2010).

Most YSOs present an IR excess, which is interpreted in terms of the presence of a circumstellar disk. We focus on the spatial distribution of the sources with excessive emission and try to elucidate the mode of star formation in IC 1396. This paper is organized as follows. In Section 2, we present the retrieval of the archived 2MASS and AKARI data, optical spectroscopy and the related data reduction. In Section 3, we explain how we explored the four subclusters that are spatially coincident with the bright rims of IC 1396. Optical identification and SED classification of the sample sources follow in Section 4. The derived results are discussed in Section 5 and summarized in Section 6.

2 DATA ACQUISITION AND ANALYSIS

2.1 Archived Data

Archived data from the 2MASS PSC were used in this work. To guarantee the reliability of the data, we employed the following strict requirements in the sample selection, which were revised based on the criteria presented by Li & Smith (2005): (1) The photometric uncertainties for each extracted

[1] *http://www.ipac.caltech.edu/2mass/releases/allsky/doc/explsup.html*

2MASS point source should be less than or equal to 0.1 mag at all three bands ($[JHK_S]_{-\mathrm{cmsig}} \leqslant 0.1$). (2) Only sources with a K_S-band signal-to-noise ratio above 15 are selected.

The sample of sources with excessive emission that were selected based on the 2MASS data was cross-identified with the AKARI (ASTRO-F) IRC PSC[2] using the simple positional correlation method. Only sources with valid S9W data (fQual_09 equals to 3) were considered. A positional tolerance of $3''$ was adopted. Based on the statistical result of the relationship between the positional offset and the numbers of counterparts detected with both the AKARI IRC PSC and 2MASS PSC, we found the chance of false matches becomes large when the tolerance radius was larger than $3''$. If more than one AKARI source was found within the tolerance radius, only the closest one was adopted. The flux of the IRC PSC sources was then converted to apparent magnitude with the following equation

$$m = -2.5 \times \log_{10}\left(\frac{F}{F_0}\right) ,$$

where F_0 (zero magnitude flux) was 56.262 ± 0.8214 Jy and 12.00 ± 0.1751 Jy for 9 μm and 18 μm bands, respectively.

2.2 Optical Spectroscopy

Spectroscopic observations of all the sample sources in IC 1396 with USNO R magnitudes brighter than 17.0 were performed on the 2.16 m optical telescope managed by the National Astronomical Observatories, Chinese Academy of Sciences (NAOC). A detector from Optomechanics Research Inc. and a 1340×400 CCD from Princeton Instruments were used in both observation runs. Low-resolution spectroscopy (with a dispersion of 200 Å mm^{-1} (4.8 Å pixel^{-1}) and a $2.5''$ slit) centered at 6300 Å was carried out on September 12, December 11, 2009, and October 3 to 4, 2010.

The spectral data were reduced following standard procedures in the software package from National Optical Astronomy Observatory called the Image Reduction and Analysis Facility (IRAF, version 2.11). The CCD reduction included bias and flat-field correction, nebula and sky background subtraction, and cosmic ray removal. Wavelength calibration was performed based on Helium-Argon lamps exposed at both the beginning and the end of the observations each night. Flux calibration of each spectrum was conducted based on observations of at least two of the KPNO spectral standards (Massey et al. 1988) each night. The atmospheric extinction was corrected by the mean extinction coefficients measured for the Xinglong Station, where the 2.16 m telescope is located, by using the Beijing-Arizona-Taiwan-Connecticut (BATC) multicolor survey.

3 CLUSTERING OF STAR FORMATION IN IC 1396

Historical studies revealed the existence of many YSO candidates and most of them are found to congregate in the densest parts of IC 1396.

Figure 1 shows the distribution of YSOs in the literature as mentioned in Section 1. Its border shows the region studied in this paper. It extends from $21^{\mathrm{h}}28^{\mathrm{m}}$ to $21^{\mathrm{h}}52^{\mathrm{m}}$ in right ascension and from 56° to 59° in declination, centered on R.A. = $21^{\mathrm{h}}40^{\mathrm{m}}00^{\mathrm{s}}$, Dec $= 57^\circ 30' 00''$ (J2000.0), which is believed to encompass the full extent of all compact subclusters.

3.1 Color-color Diagram

The 2MASS database contains more than half a million photometric detections in this region. We narrowed down the catalog to 108 966 sources using our selection criteria mentioned above.

A 2MASS JHK_S color-color (C-C) diagram is widely used to select sources with excessive IR emissions.

[2] *http://darts.isas.jaxa.jp/astro/akari/cas.html*

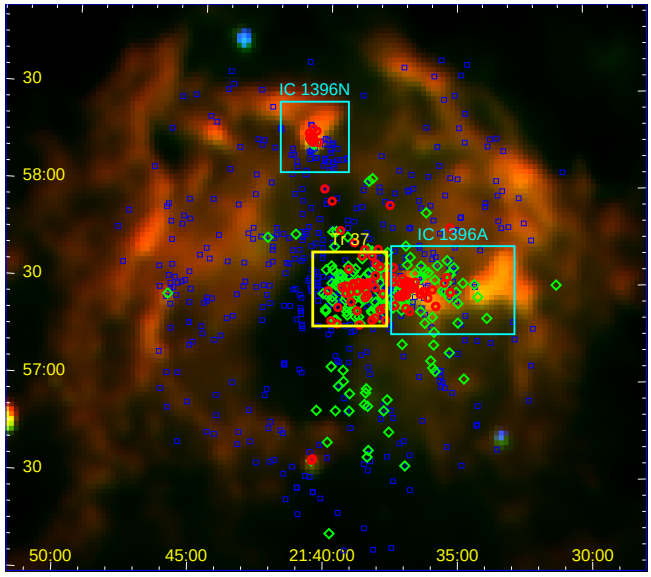

Fig. 1 Distribution of known YSOs in IC 1396. Historical studies were limited to the densest parts: IC 1396A, IC 1396N and Tr 37. Red circles indicate weak–line T Tauri stars and CLASS II/III sources, while green diamonds indicate classical T Tauri stars and CLASS I sources. The background image is trichromatic and generated from IRAS 25 (*blue*), 60 (*green*), and 100 (*red*) μm maps.

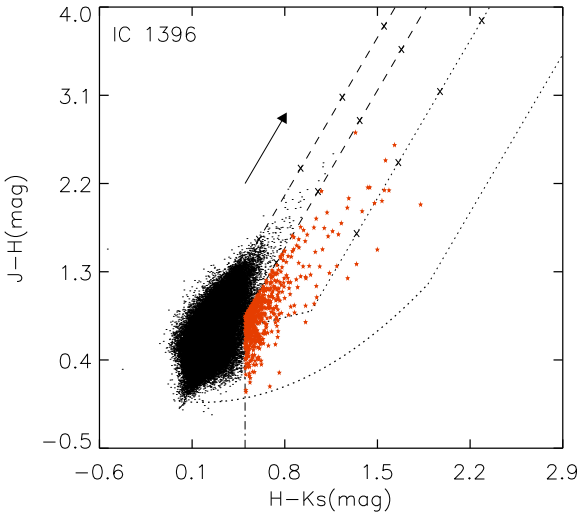

Fig. 2 $(J-H)$ versus $(H-K_S)$ C-C diagram of IC 1396. The sample sources are denoted as dots. Selected IR sources with excessive emission are labeled in red. Black solid lines represent the loci of the MS dwarfs and giant stars (Bessell & Brett 1988). Two parallel dashed lines define the reddening band for normal stars. The arrow shows a reddening vector of $A_v = 5$ mag (Rieke & Lebofsky 1985). The left dotted line indicates the loci of dereddened T Tauri stars (Meyer et al. 1997) and their reddening band boundary. The right dotted line indicates the loci of dereddened Herbig Ae/Be stars (Lada & Adams 1992) and their reddening direction. Crosses are plotted over the figure with an interval corresponding to 5 mag of visual extinction.

Figure 2 shows the C-C diagram for IC 1396. All the 2MASS sources that match our criteria are put into the JHK_S C-C diagram and denoted as dots. We define 598 objects as YSO candidates whose colors place them below the right line of the normal star reddening band and $H - K_S > 0.5$. Those sources are selected because they possess intrinsic color excesses likely originating from emission of circumstellar dust, commensurate with their embedded nature. The color distinction helps to eliminate foreground field stars and narrow the sample of YSO candidates.

3.2 Surface Density Distribution

The distribution showing the scale of all the 2MASS sources and YSO candidates is presented in Figure 3. On the scale of the entire IC 1396, significant enhancement of stellar density in the center region is easily distinguished in the stellar surface density distribution of all the 2MASS sources (in Fig. 3 (a)). There are about 59 sources covering an area of 0.0025 deg^2 in the densest region, which coincides with the young open cluster Tr 37. However, we cannot find the structure of the H II region in this panel.

In panel (b), the spatial distribution of the YSO candidates, representing the four densest regions, are revealed. Compared with the 100 μm image from IRAS, subclusters A, B, and C correspond to the bright rims (Sugitani et al. 1991) marked in Figure 3 (c), while the central subcluster D is at the location of open cluster Tr 37. Regions A and B correspond to IC 1396 A and IC 1396 N, centered at $21^{\rm h}36^{\rm m}54^{\rm s}$, $57^\circ33'00''$ (J2000.0) and $21^{\rm h}40^{\rm m}42^{\rm s}$, $58^\circ15'14''$ (J2000.0), respectively. Region C is the most scattered one, and contains several stellar aggregates. Among them the most compact and biggest one is centered at $21^{\rm h}46^{\rm m}15^{\rm s}$, $57^\circ25'00''$ (J2000.0). Compared to the outer regions A, B, and C, region D is hardly found in the ISSA image, because it has already lost the protection of dust in IR bands from the radiation of the exciting star HD 206267. However, it still contains a number of YSO candidates.

4 IDENTIFICATION AND CLASSIFICATION OF EXCESSIVE EMISSION SOURCES IN IC 1396

To further investigate the scenario of star formation in IC 1396, AKARI IRC PSC was employed. Mid-IR data are more sensitive to cold dust in the circumstellar disks and are essential for fitting an SED. All the sources with excessive emission selected based on the 2MASS C-C diagram were cross-identified with the AKARI IRC PSC, which resulted in a sample of 44 sources. Except for the four classical Be stars (CBe) and two carbon stars identified with SIMBAD, all of the sample sources are presented in Table 1, which presents the ID numbers of these sources, 2MASS PSC coordinates (J2000), USNO R magnitudes, EW[Hα], EW[Li], spectral types, and classification based on SEDs.

4.1 Optical Identification

To identify and classify the sample sources, optical spectra were obtained with the 2.16 m optical telescope of NAOC. Combined with equivalent width measurements of Hα (EW[Hα]), all the sources with spectral types earlier than F5 and Hα in emission were identified as Herbig Ae/Be stars (HAeBe). Classical T Tauri stars (CTTSs) are, on the other hand, selected based on the criteria that a CTTS shows an EW[Hα] value greater than 3 Å for K0–K5 stars, an EW[Hα] value greater than 10 Å for K7–M2.5 stars, an EW[Hα] value greater than 20 Å for M3–M5.5 stars, and an EW[Hα] value greater than 40 Å for M6–M7.5 stars (White & Basri 2003). However, stars with values of EW[Hα] below these levels are not necessarily weak-line T Tauri stars (WTTSs) as they share very similar SEDs with MS stars. Further identification based on the detection of Li I 6707 Å absorption is necessary (Martín 1998). Except for four CBes, 23 stars out of the 33 observed sources are identified as YSOs due to the presence of prominent Hα emission. Among these, there are five CTTSs, seven HAeBes, and eight WTTSs. For the remaining three, no prominent Li I absorption is detected

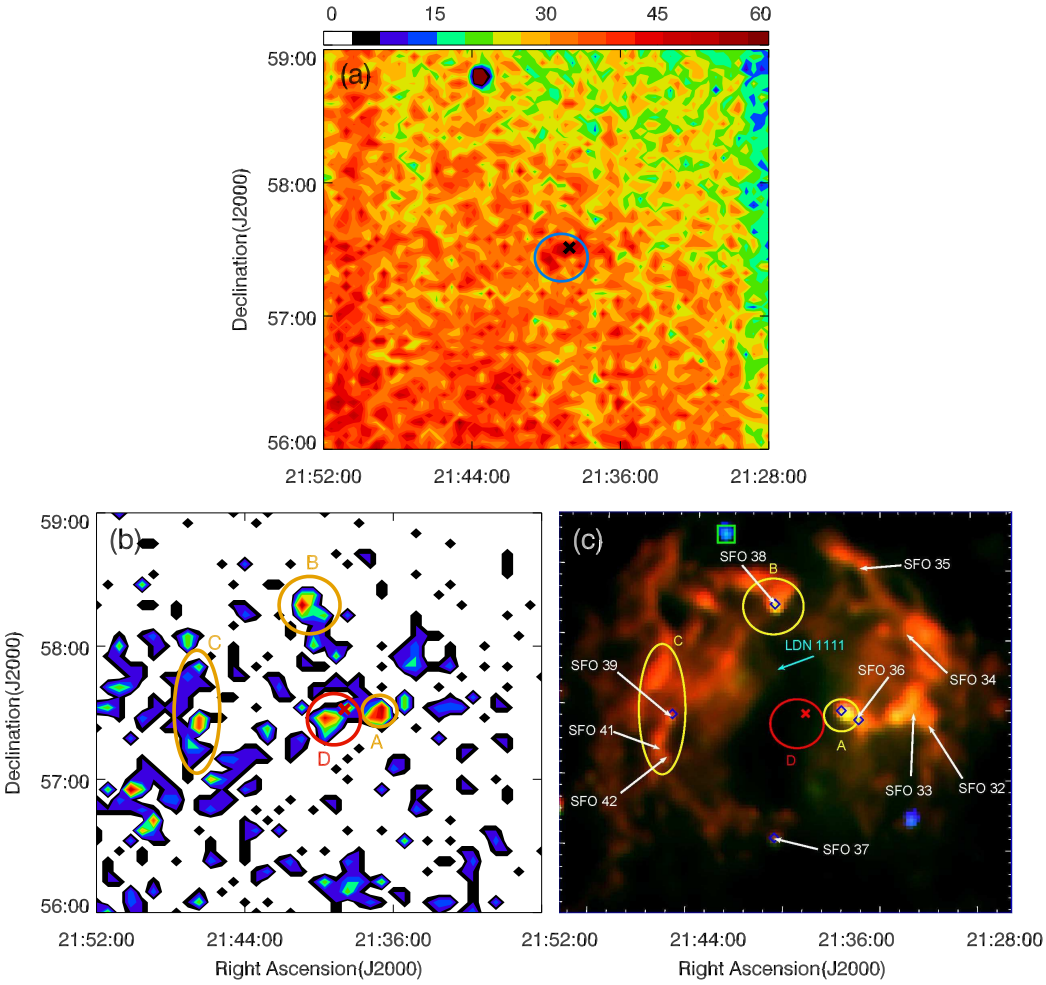

Fig. 3 (a) Surface density distribution of the 2MASS sources toward IC 1396. The densest region at the center marked with a circle is consistent with the position of the open cluster Tr 37, and the cross indicates HD 206267 at R.A.= $21^{\rm h}38^{\rm m}57^{\rm s}$, Dec= $+57^{\circ}29'20''$(J2000). The hole near the top left corner is formed by a saturated bright source, which is marked with a green box in panel (c). The color bar indicates the number of sources in every 0.0025 square degrees. (b) Spatial distribution of 598 2MASS sources with excessive emission. A red cross indicates the exciting star HD 206267. Yellow circles mark the four densest regions of the YSO candidates, which harbor active star formation. (c) Trichromatic image of IC 1396 generated from IRAS 25 (*blue*), 60 (*green*), and 100 (*red*) μm maps. Bright rims (Sugitani et al. 1991) and BOLOCAM data (*blue diamonds*) are plotted. A red cross indicates the main exciting source HD 206267.

because of the low signal to noise ratio in the optical spectra. However, the existence of strong Hα emission and excessive emission in IR seems to corroborate their nature as YSOs.

Figure 4 illustrates the sample spectra of WTTS and CTTS. Among the sample of 33 observed sources, 27 are found to be strong Hα emission stars. Three HAeBes, one CTTS and 13 WTTSs are newly discovered in IC 1396.

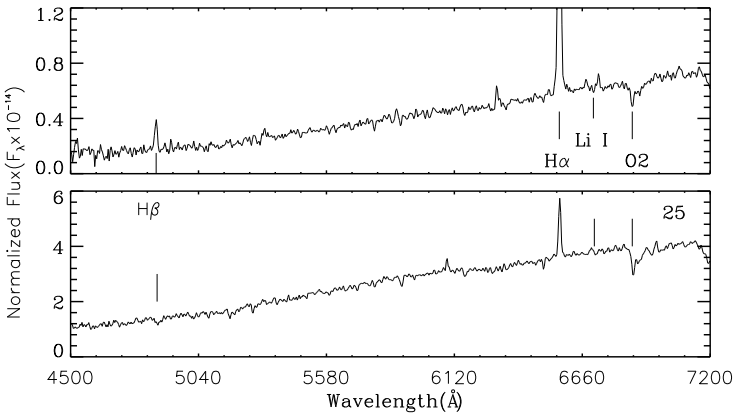

Fig. 4 Typical WTTS (No. 21) and CTTS (No. 25) spectra in IC 1396, showing the Balmer series in emission (mainly Hα) and Li absorption at 6707 Å.

4.2 Classification Based on SED Fitting

We tried to determine the evolutionary status of the sample sources based on their SEDs. A grid of 200 000 YSO models was developed (Robitaille et al. 2006), spanning a wide range of evolutionary stages for different stellar masses, to model the SED from optical to millimeter wavelengths. This archive provides a linear regression tool which can select all model SEDs that fit the observed SED better than a specified χ^2 (Robitaille et al. 2006).

On the basis of the "four stage" star formation scenario proposed by Shu et al. (1987), Lada (1987) developed a widely used classification scheme for YSOs, primarily based on their SEDs. With an evolutionary sequence from early type to late type, YSOs were divides into sets denoted by CLASS I to III. Robitaille et al. (2006) presented a classification scheme that is essentially analogous to the class scheme, but refers to the actual evolutionary stage of the object based on physical properties like disk mass and envelope accretion rate. However, in view of the differences between observable and physical properties, ages fitted by the tool and the slope of its near/mid-IR SED are our primary standard of reference. CLASS I refers to those objects that have age $\approx 10^5$ yr and slope$_{\rm near/mid-IR}$ >0, CLASS II refers to age $\approx 10^6$ yr and slope$_{\rm near/mid-IR}$ $\leq$0, and CLASS III is for objects whose SED is similar to a blackbody spectrum.

Collections of multi-wavelength online data were used for SED fitting. Besides 2MASS PSC and AKARI IRC/FIS data, we used: (1) BVR photometry from the Naval Observatory Merged Astrometric Dataset (NOMAD); (2) the mid-IR A (8.28 μm), C (12.13 μm) and D (14.65 μm) provided by the MSX6C IR PSC; (3) photometry of the far-IR IRAS Point Sources at 12, 25, 60 and 100 μm; (4) IRAC and MIPS photometry at 3.6, 4.5, 5.8, 8 and 24 m for a handful of sources. As a result, we end up fitting the SEDs of a photometric catalog with a large coverage in wavelength. Though several sources lack data at far-IR bands, it is still crucial to investigate the PMS nature of sample sources in terms of IR excess in their SEDs.

The evolutionary status of all the YSO candidates listed in Table 1 is further confirmed by results of the SED fitting.

Figure 5 illustrates the SED of the sources from CLASS I and CLASS II in the sample. Based on the SED fitting, all the sample sources indicate masses of $< 5\ M_\odot$ and ages of < 3 Myr, which is in good agreement with the results of Nakano et al. (2012) and Choudhury et al. (2010).

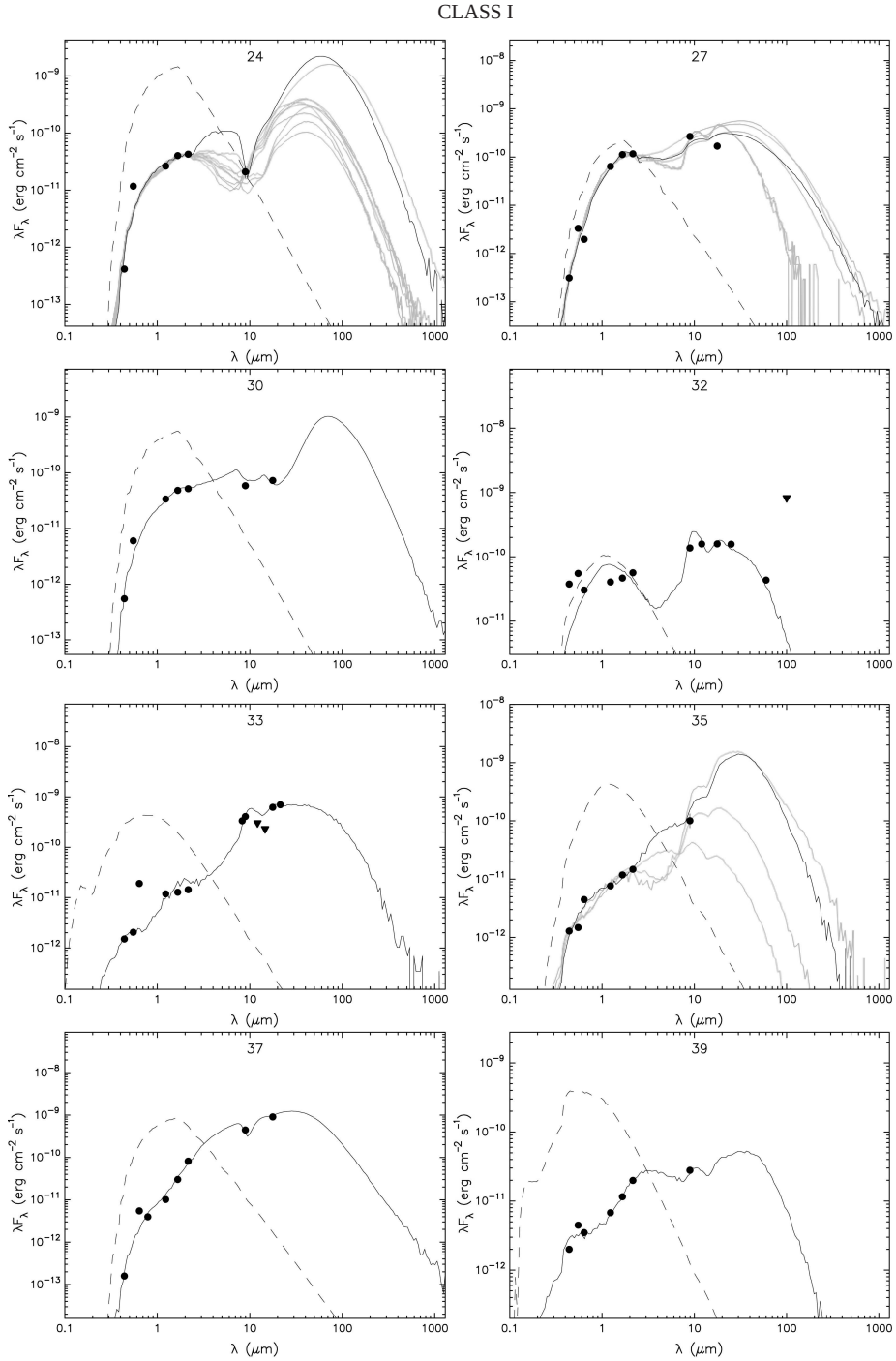

Fig. 5 Results of the SED fitting for the sample sources. The solid black curve gives the best model fitting of the data points with the smallest χ^2. The gray curve represents the other potential model fitting results with $\chi^2/N - \chi^2_{\rm best}/N < 3$. The dashed curve indicates the photosphere that is used as input for the radiative transfer code. The black dots show the measured fluxes currently available. The filled upside-down triangles indicate the upper limit of detection in each of the corresponding bands.

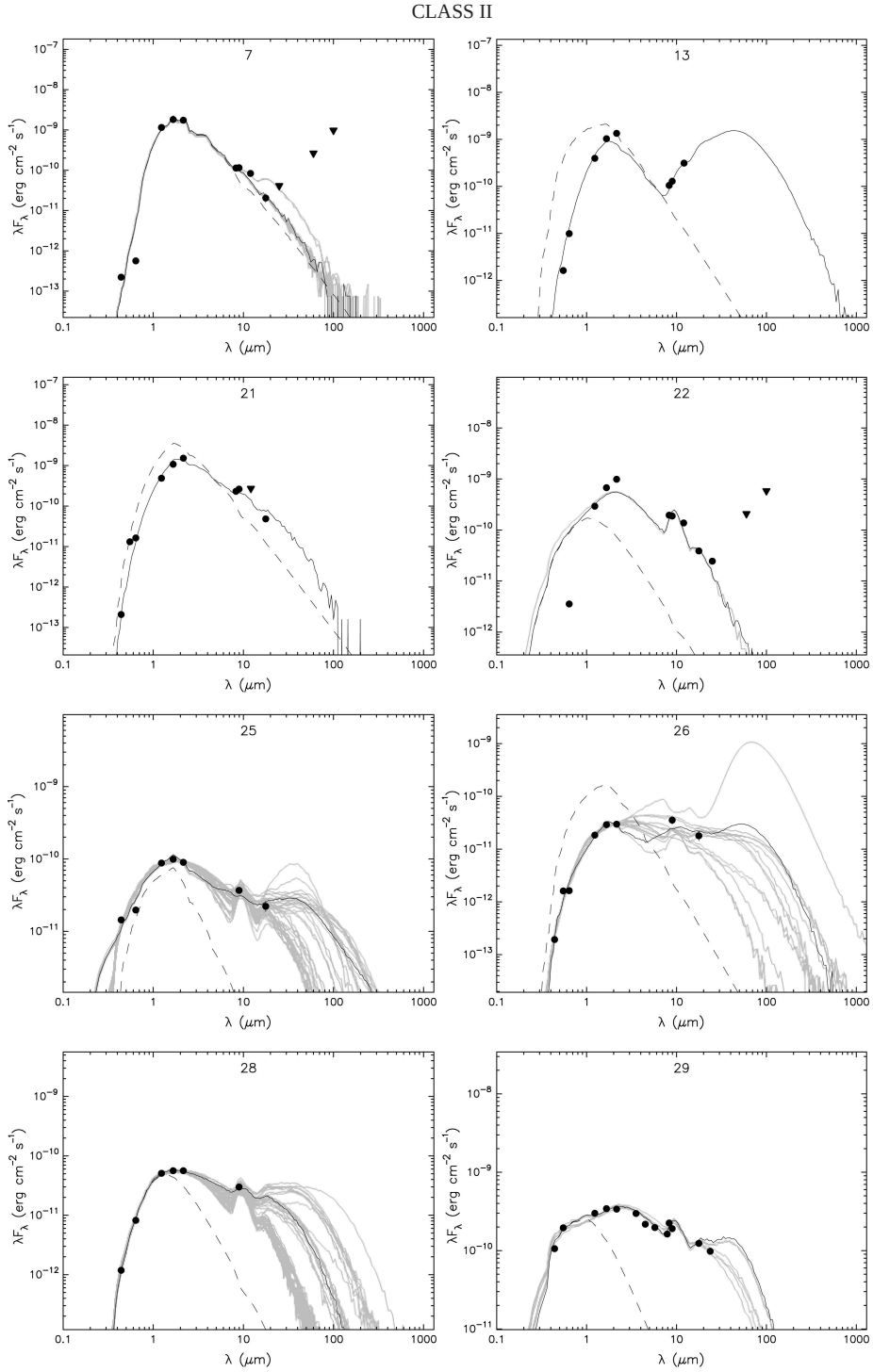

Fig. 5 *Continued.*

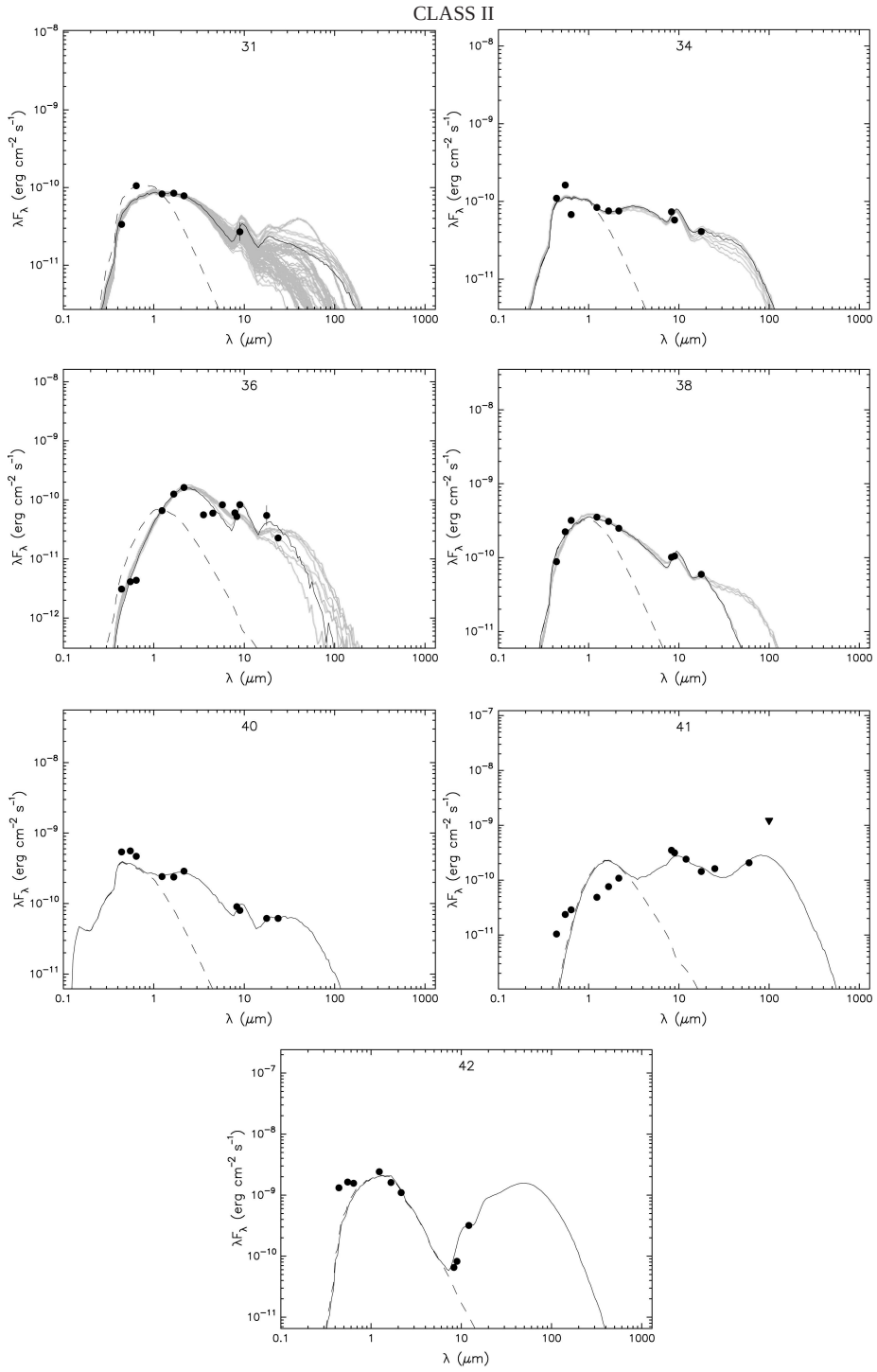

Fig. 5 *Continued.*

Table 1 Optical Identification and Classification of the Sample Sources toward IC 1396

ID	R.A. (J2000)	Dec. (J2000)	R	EW		Sp.	Class		
	[h m s]	[° ′ ″]	[mag]	[Hα]	[Li]		Spectra	C-C diagrams	SEDs
1*	21 42 33.57	58 14 39.11	12.21	−12.1	...	B2	CBe	CBe	...
2*	21 48 21.16	56 09 20.15	12.41	−9.05	...	B4	CBe	CBe	...
3*	21 36 59.63	58 08 24.72	12.21	−27.9	...	B3	CBe	CBe	...
4	21 42 24.16	57 44 09.96	14.77	−4.99	...	O9	CBe	CBe	...
5	21 29 23.95	56 19 49.43	14.73	−2.15	0.57	M4	WTTS	WTTS	III
6	21 47 15.45	56 23 45.95	15.63	−6.18	0.08	M4	WTTS	WTTS	III
7	21 43 33.09	57 25 25.31	24.61	...	...	...	...	WTTS	II
8	21 46 35.97	57 49 31.79	18.07	...	...	...	...	WTTS	III
9*	21 43 08.73	57 11 58.20	16.1	−20.5	2.02	M7	WTTS	WTTS	III
10*	21 34 15.59	56 18 11.88	16.1	−1.97	0.35	M6	WTTS	WTTS	III
11*	21 40 03.86	57 42 18.71	17.41	...	...	M3	...	WTTS	III
12*	21 45 34.12	56 23 42.72	16.81	...	...	M2	...	WTTS	III
13*	21 32 44.54	56 21 25.56	16.1	−4.56	0.86	M7	WTTS	WTTS	II
14	21 46 41.23	57 00 10.80	14.97	−3.38	0.48	M5	WTTS	WTTS	III
15*	21 39 10.63	57 06 47.16	16.01	−2.36	0.53	M4	WTTS	WTTS	III
16*	21 50 21.50	56 53 10.32	20.61	...	...	...	...	WTTS	III
17	21 43 16.43	56 01 42.60	14.3	−10.2	...	M9	WTTS	WTTS	III
18	21 42 47.61	58 57 20.52	13.11	...	...	M8	...	WTTS	III
19	21 42 12.04	58 25 12.00	26.41	...	...	M8	...	WTTS	III
20*	21 39 06.38	57 43 51.60	16.95	−14.1	...	M7	WTTS	WTTS	III
21	21 38 42.31	57 30 27.71	16.41	−12.9	...	M4	WTTS	WTTS	II
22	21 39 09.33	58 38 53.87	16.41	...	...	M7	...	WTTS	II
23*	21 43 51.47	58 15 07.92	19.73	...	...	...	...	WTTS	III
24*	21 48 11.75	57 59 41.64	15.7	−86.3	0.84	F8	CTTS	CTTS	I
25	21 36 49.56	57 48 23.39	14.85	−6.52	0.02	G6	CTTS	CTTS	II
26	21 45 05.87	57 11 38.75	18.21	...	...	...	...	CTTS	II
27	21 34 19.63	57 30 02.52	15.7	−45.1	0.23	F7	CTTS	CTTS	I
28	21 35 43.60	57 03 47.52	14.81	−2.92	0.23	K3	WTTS	CTTS	II
29*[1]	21 38 17.32	57 31 22.07	13	−14.5	0.11	F9	CTTS	CTTS	II
30	21 46 00.26	57 23 09.60	18.35	...	...	...	...	CTTS	I
31	21 45 54.07	57 28 18.48	14.4	−9.65	0.1	K4	CTTS	CTTS	II
32	21 30 22.84	58 28 51.95	14.37	−40.5	0.31	A9	HAeBe	HAeBe	I
33	21 49 38.27	56 54 36.72	15.7	−141	0.12	F2	HAeBe	HAeBe	I
34	21 35 19.15	57 36 38.15	15.21	−6.98	0.01	A8	HAeBe	HAeBe	II
35*	21 29 58.03	56 28 50.51	17.5	...	...	...	...	HAeBe	I
36[2]	21 36 39.14	57 29 53.16	17	...	...	...	...	HAeBe	II
37	21 46 07.12	57 26 31.91	17.21	...	...	...	...	HAeBe	I
38	21 45 02.32	56 49 51.60	14.21	2.35	0.25	F9	...	HAeBe	II
39	21 45 24.55	57 55 49.08	16.1	−11.1	0.79	F3	HAeBe	HAeBe	I
40	21 38 08.44	57 26 47.75	14.15	−5	0.1	A2	HAeBe	HAeBe	II
41	21 33 17.78	57 48 13.31	14.53	−62.6	0.13	F3	HAeBe	HAeBe	II
42	21 51 00.57	56 21 19.44	10.24	−43.1	...	F3	HAeBe	HAeBe	II
43	21 43 56.92	58 35 45.95	18.17	...	...	...	...	Carb.	...
44	21 38 28.34	57 08 19.32	16.91	...	...	M7	...	Carb.	...

* Sources not detected with IRC 18 μm; [1] IC 1396 A: θ – identified as CTTS from Sicilia-Aguilar et al. (2006);
[2] Identified as a CLASS II source from Reach et al. (2009).

5 DISCUSSION

Marschall et al. (1990) suggested that stars from the first generation in IC 1396 reached the main sequence 7 Myr ago, and Sicilia-Aguilar et al. (2005) gave an age of 4 Myr for the young open cluster Tr 37 based on optical photometry and theoretical isochrones. The expansion of the H II region has created a swept-up shell and resulted in a compressed molecular ring around its periphery (Nakano et al. 2012). Based on the physical scale of the ring, Patel et al. (1995) suggested a dynamical age

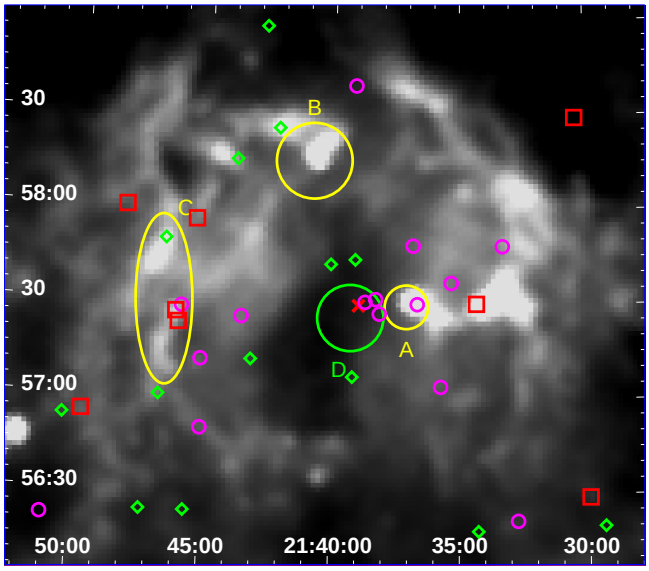

Fig. 6 Distribution of the sample sources classified with SEDs. CLASS I, II and III sources are indicated with red boxes, magenta circles and green diamonds, respectively. The red cross represents the exciting star HD 206267. The background image is the IRAS 100 μm map of IC 1396. The yellow circles, yellow oval and green circle represent the same areas as in Figure 3.

of 2–3 Myr. A number of Hα stars with ages younger than 3 Myr were detected by Nakano et al. (2012). They are spatially associated with the bright rims. Based on the disparity in ages for various groups of stars, we tentatively suggest a scenario of sequential or episodic star formation in IC 1396.

Figure 6 presents the IRAS 100 μm mosaic of IC 1396, on which the sample sources, classified based on SEDs, are overlaid with different symbols. Although the number of CLASS I sources identified in this study is small, all the CLASS I sources are found to be located in the bright rims or the molecular ring of IC 1396, while YSOs at later evolutionary stages (e.g. CLASS III) are congregated in the central part of the H II region. Furthermore, all the identified CLASS I and CLASS II sources are located in the surrounding sub-clusters rather than the central open cluster Tr 37. All these are consistent with episodic behavior of star and cluster formation in this H II region. A direct consequence of episodic star formation is that different generations of stars occupy distinct regions.

A spatial gap seems to exist between the central open cluster and the surrounding subclusters in both the optical and the near-IR, which is believed to be the result of discontinuous star formation in this region. To further investigate the interstellar materials within the gap, Herschel SPIRE data are employed. As shown in Figure 3 (c), there is an optically dark cloud between Tr 37 and subcluster B. This dark cloud was cataloged by Lynds (1962) as LND 1111, which shows a large amount of extinction both in the optical and the near-IR. The right panel of Figure 7 presents a composite image of LND 1111, which was compiled with the SPIRE 250 μm (blue), 350 μm (green), and 500 μm (red) imaging data. It is evident that the dark globule corresponding to LND 1111 in the digitized sky survey 2 blue band image (left panel in Fig. 7) is bright in emission in the far-IR. This indicates the existence of a large amount of cold dust. The overlaid contours generated based on the Herschel SPIRE image indicate the presence of two far-IR cores, which are likely to be nurseries of a new generation of stars. Therefore, we infer that new generations of stars are being formed in

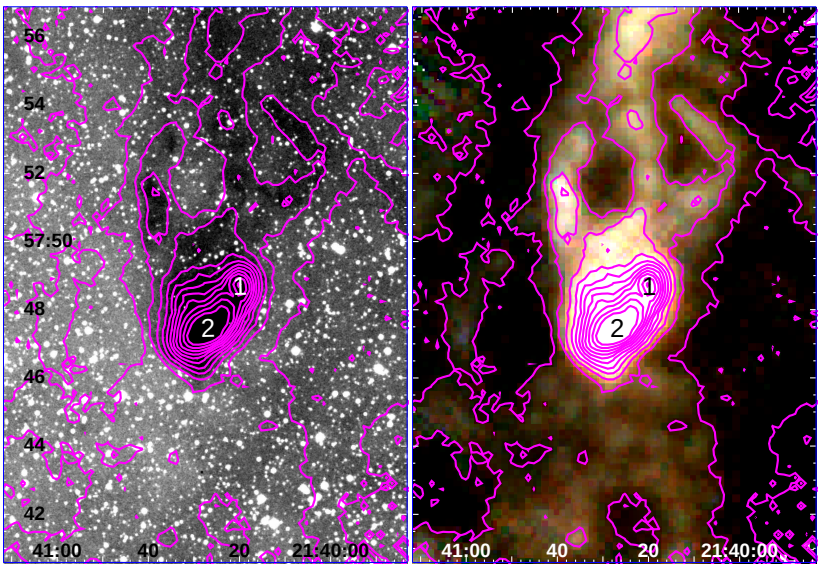

Fig. 7 *Left*: digitized sky survey 2 blue band image of LDN 1111. *Right*: color composite image of the dark cloud LDN 1111 in 250 μm (*blue*), 350 μm (*green*) and 500 μm (*red*). Magenta contours in both images are generated from the Herschel SPIRE image in the 500 μm band.

IC 1396, and star formation in this region is not continuous but rather sequential or episodic. Further investigations are necessary to explore if new generations of star and cluster formation in IC 1396, both in the vacant bubble and the interface of the HII region, have a triggered origin or not.

6 SUMMARY

We present a comprehensive study of the H II region IC 1396 and its star formation activity. Excessive emission sources are selected based on the archived 2MASS data and their cross-identification with AKARI IRC PSC. SED fittings are employed to classify the IR sources. In the target region, eight CLASS I, 15 CLASS II and 15 CLASS III sources were identified. Optical identification of the sample sources with USNO R magnitudes brighter than 17.0 corroborates results from the classification of the IR sources based on SED fitting. Among the sub-sample of 33 observed sources, 27 are found to present strong Hα emission. However, three HAeBes, one CTTS and 13 WTTSs are newly discovered.

The spatial distribution of the IR sources with excessive emission that were selected based on their 2MASS colors reveals four sub-clusters toward IC 1396. One is spatially associated with the open cluster Tr 37 that hosts the exciting source for the H II region. The other three are found to be spatially coincident with the bright rims of the surroundings. All the identified CLASS I and CLASS II sources are found to be located in the surrounding sub-clusters rather than the central young open cluster Tr 37, which is primarily a congregation of CLASS III sources. The surrounding sub-clusters are thus believed to be much younger due to the spatial distribution of IR sources at different evolutionary stages. This is consistent with a scenario of sequential star formation in this region. Imaging data of a dark patch in IC 1396 from Herschel SPIRE indicate the presence of two far-IR cores, which are likely to be evidence for new generations of star formation. Therefore, we infer that star formation in IC 1396 was not continuous but rather sequential and/or episodic.

Acknowledgements We very much appreciate the helpful comments and suggestions from the referee. This work employed data from the 2MASS, AKARI and other databases. Our investigation is supported by funding from the National Natural Science Foundation of China (Grant Nos. 11073027 and 11003021) and the Department of International Cooperation of the Ministry of Science and Technology of China (Grant No. 2010DFA02710).

References

Barentsen, G., Vink, J. S., Drew, J. E., et al. 2011, MNRAS, 415, 103
Bessell, M. S., & Brett, J. M. 1988, PASP, 100, 1134
Choudhury, R., Mookerjea, B., & Bhatt, H. C. 2010, ApJ, 717, 1067
Froebrich, D., & Scholz, A. 2003, A&A, 407, 207
Froebrich, D., Scholz, A., Eislöffel, J., & Murphy, G. C. 2005, A&A, 432, 575
Getman, K. V., Feigelson, E. D., Garmire, G., Broos, P., & Wang, J. 2007, ApJ, 654, 316
Ishihara, D., Onaka, T., Kataza, H., et al. 2010, A&A, 514, A1
Kawada, M., Baba, H., Barthel, P. D., et al. 2007, PASJ, 59, 389
Kun, M., Kiss, Z. T., & Balog, Z. 2008, in Handbook of Star Forming Regions: The Northern Sky, ed. B. Reipurth (San Francisco, CA: ASP), 136
Lada, C. J. 1987, in Star Forming Regions, IAU Symposium, 115, eds. M. Peimbert & J. Jugaku (Dordredcht: Reidel), 1
Lada, C. J., & Adams, F. C. 1992, ApJ, 393, 278
Lada, C. J., & Lada, E. A. 2003, ARA&A, 41, 57
Li, J. Z., & Smith, M. D. 2005, A&A, 431, 925
Lynds, B. T. 1962, ApJS, 7, 1
Marschall, L. A., Karshner, G. B., & Comins, N. F. 1990, AJ, 99, 1536
Martín, E. L. 1998, AJ, 115, 351
Massey, P., Strobel, K., Barnes, J. V., & Anderson, E. 1988, ApJ, 328, 315
Matthews, H. E., Haslam, C. G. T., Hills, D. L., & Salter, C. J. 1980, A&A, 88, 285
Mercer, E. P., Miller, J. M., Calvet, N., et al. 2009, AJ, 138, 7
Meyer, M. R., Calvet, N., & Hillenbrand, L. A. 1997, AJ, 114, 288
Nakano, M., Sugitani, K., Watanabe, M., et al. 2012, AJ, 143, 61
Neri, R., Fuente, A., Ceccarelli, C., et al. 2007, A&A, 468, L33
Onaka, T., Matsuhara, H., Wada, T., et al. 2007, PASJ, 59, 401
Patel, N. A., Goldsmith, P. F., Snell, R. L., Hezel, T., & Xie, T. 1995, ApJ, 447, 721
Reach, W. T., Rho, J., Young, E., et al. 2004, ApJS, 154, 385
Reach, W. T., Faied, D., Rho, J., et al. 2009, ApJ, 690, 683
Rieke, G. H., & Lebofsky, M. J. 1985, ApJ, 288, 618
Robitaille, T. P., Whitney, B. A., Indebetouw, R., Wood, K., & Denzmore, P. 2006, ApJS, 167, 256
Shu, F. H., Adams, F. C., & Lizano, S. 1987, ARA&A, 25, 23
Sicilia-Aguilar, A., Hartmann, L. W., Hernández, J., Briceño, C., & Calvet, N. 2005, AJ, 130, 188
Sicilia-Aguilar, A., Hartmann, L. W., Fürész, G., et al. 2006, AJ, 132, 2135
Simonson, S. C., III 1968, ApJ, 154, 923
Sugitani, K., Fukui, Y., & Ogura, K. 1991, ApJS, 77, 59
Weikard, H., Wouterloot, J. G. A., Castets, A., Winnewisser, G., & Sugitani, K. 1996, A&A, 309, 581
Wendker, H. J., & Baars, J. W. M. 1980, A&A, 89, 180
White, R. J., & Basri, G. 2003, ApJ, 582, 1109